Estimating the surface relaxivity as a function of pore size from NMR T2 distributions and micro-tomographic images

Francisco Benavides[a)1)], Ricardo Leiderman[a)], Andre Souza[b)], Giovanna Carneiro[b)c)],Rodrigo Bagueira[c)]

a) Computer Science Department, Fluminense Federal University, Av. Gal. Milton Tavares de Souza, s/no, Niterói, RJ, Brazil, 24210-346. fbenavides@id.uff.br; leider@ic.uff.br.

b) Schlumberger Brazil Research & Geoengineering Center, Rua Paulo Emidio Barbosa, 485, quadra 7B, Parque Tecnologico do Rio de Janeiro, Rio de Janeiro, RJ, Brazil, CEP 21941-907. ASouza19@slb.com; giovannafc@gmail.com

c) Institute of Chemistry, Fluminense Federal University, Outeiro de São João Batista, s/no, Niterói, RJ, Brazil, 24020-141. rbagueira@vm.uff.br.

1)Author to whom correspondence should be addressed. Electronic mail: fbenavides@id.uff.br

Abstract

In the present work, we formulate and solve an inverse problem to recover the surface relaxivity as a function of pore size. The input data for our technique are the T_2 distribution measurement and the micro-tomographic image of the rock sample under investigation. We simulate the NMR relaxation signal for a given surface relaxivity function using the random walk method and rank different surface relaxivity functions according to the correlation of the resulting simulated T_2 distributions with the measured T_2 distribution. The optimization is performed using genetic algorithms and determines the surface relaxivity function whose corresponding simulated T_2 distribution best matches the measured T_2 distribution. In the proposed methodology, pore size is associated with a number of collisions in the random walk simulations. We illustrate the application of the proposed method by performing inversions from synthetic and laboratory input data and compare the obtained results with those obtained using the uniform relaxivity assumption.

Keywords: Surface relaxivity; NMR magnetization decay; Digital Petrophysics; Random walk; Pore size distribution.

1 - Introduction

$^{1}\mathrm{H}$ Nuclear Magnetic Resonance (NMR) is a powerful tool for studying reservoir rock properties, based on the responses of protons in fluid molecules filling the formation pore space. Porosity, pore size distribution, permeability, capillary pressure curves and wettability are examples of important petrophysical deliverables that can be accessed *via* laboratory and field (downhole and surface) NMR realizations (Coates et al., 1999)(Dunn et al., 2002).

According to the basic theory, the NMR transversal relaxation rates $(1/T_2)$ of protons in molecules of the wetting phase can be enhanced by contact or quasi-contact interactions with the solid/fluid interfaces. In the limit of the fast diffusion regime, the solid-fluid interaction is the dominant relaxation mechanism and the relaxation rate of a fluid occupying the pore space can be approximated by (Brownstein and Tarr, 1979):

$$\frac{1}{T_2} = \rho_2 \left(\frac{S_p}{V_p}\right) = \rho_2 \frac{c}{R_p} \quad , \tag{1}$$

where (S_p/V_p) is the ratio of surface area to pore volume; ρ_2 (ρ, from now on) is the surface relaxivity, a proportionality constant that characterizes the strength of relaxation induced by the solid/fluid interfaces; R_p is the pore radius and c is the shape factor $(1,2$ and 3 for planar, cylindrical and spherical pores, respectively). When an estimate for the surface relaxivity parameter is available, the measured relaxation time distribution can be converted into a pore size distribution using the equation above. In the formation evaluation context, the pore size distribution is one of the distinctive NMR deliverables when compared to the other available geophysical methods.

58 The importance of accessing surface relaxivity values for improving the accuracy of
59 NMR deliverables is described in several papers, such as for example in (Souza et al.,
60 2013), where the authors demonstrated how to calibrate the relaxation term of a classical
61 NMR permeability model to improve its performance. According to (Saidian and Prasad,
62 2015), there are three primary types of methods to estimate the surface relaxivity:

63 i. Iterative variation to match NMR relaxation times with independent measurements
64 of pore or throat size distribution;
65 ii. Estimations using rock surface area;
66 iii. Estimations based solely on NMR measurements;

67 All of them rely upon the assumption that the surface relaxivity can be represented by a
68 uniform value. However, as stated in (Keating and Knight, 2012), it is highly unlikely that
69 all the pore surfaces in a sedimentary rock sample have the same relaxivity value.

70 In (Arns et al., 2006), the authors cite multiple physiochemical factors that cause the
71 surface relaxivity to vary in sedimentary formations. Considering the rock formation
72 depositional, diagenetic, and hydrocarbon-filling mechanisms, it is a reasonable
73 conjecture that, for at least some cases, some of these factors may be related to pore
74 size. For example, we can cite mixed wettability reservoirs in which the wettability for
75 larger pores has been altered to oil-wet due to heavier oil fraction deposition, while the
76 wettability in smaller pores has remained unaltered (water-wet) (Looyestijn and Hofman,
77 2006). In this case, the surface relaxivity would be larger for the smaller pores and vice
78 versa. Another example we can cite are rock formations in which clay and heavy minerals
79 have been deposited differently according to the pore size. In fact, in (Boggs, 2009) the
80 author mentions that for sandstones, smaller pores will more likely contain higher

amounts of clay mineral, while larger pores will have more quartz grains in their surroundings. In this case, again, the surface relaxivity would be larger for the smaller pores. The results presented in (Liu et al., 2014) corroborate what is stated here; as for the investigated sandstone, the authors observed that the surface relaxivity was larger for the smaller pores, although they offered no justification for such behavior. In the author's own words: "The slope of the result in sandstone varies in the different pore regimes, which implies heterogeneous surface properties in the pores. The surface relaxivity was estimated to be around 30 μm/s in the pore length ranging from 10 μm to 70 μm, and was continuously increasing in the pores smaller than 10 μm". To the best of our knowledge, this is the first and only study reported in the literature that attempted to investigate the surface relaxivity variation in rock samples. At this point, we would like to mention that the results obtained in the present work for the investigated carbonate also indicated a clear tendency of the surface relaxivity to vary with pore size.

Based on the above concept, in this study we formulate and solve an inverse problem to recover the surface relaxivity as a function of pore size. To the best of our knowledge, there is no work reported in the literature treating the same inverse problem. The input data for our technique are the T_2 distribution measurement and the micro-tomographic image of the rock sample under investigation, and the inverse problem under consideration is precisely that of (iteratively) finding the surface relaxivity function whose corresponding T_2 distribution best matches the T_2 distribution measurement. To that end, we simulate the transversal NMR relaxation signal (and the corresponding T_2 distribution) for a given surface relaxivity function using a random walk implementation developed in house and that runs in the sample tomographic image, and rank different surface

relaxivity functions based on the correlation of the resulting simulated T_2 distributions with the reference (measured) T_2 distribution. The heuristic method used for the optimization is genetic algorithms. The proposed methodology is suitable for the experimental characterization of surface relaxivity on preserved pores and also provides the ability to probe the surface alterations that are chemically induced by alkaline, surfactant and polymer flooding in enhanced oil recovery (EOR) studies.

The continuation of this article is structured as follows: In Section 2 we formulate the inverse problem and present the solution strategy, where we describe how we perform the NMR relaxation simulation from digital images and introduce the concept of associating the number of collisions in the random walk simulations to pore size. In Section 3, we illustrate the application of the presented method performing inversions from (noisy) synthetic and laboratory input data, discuss the obtained results, and compare them to those obtained with the uniform relaxivity assumption. Then, we conclude in Section 4.

2 – Methods

We start this section by highlighting that what we call “inverse problem” in the present work is the whole problem of recovering the surface relaxivity as a function of pore size. Likewise, what we call “inversion procedure” (or simply “inversion”) is the entire computational process to recover the surface relaxivity as a function of pore size. This is not to be confused with the inverse Laplace transform employed to obtain the T_2 distribution from the (simulated) magnetization exponential decay.

2.1 NMR decay simulation

We use the voxel-based approach of the random walk method (RW) to simulate the NMR T_2 magnetization decay $M(t)$ in a rock sample. The sample is described by a 2D or 3D digital image in which the pores are identified in the discrete picture elements that can be voxels or pixels. The value of $M(t)$ decays according to two relaxation mechanisms: non-uniform and bulk relaxation. The fluid's contact with the pore space solid walls produces non-uniform relaxation $M_{NU}(t)$. The bulk relaxation is a fluid property and does not depend on any property of the confining formation. It is given by $M_B(t) = e^{-t/T_{2,B}}$, where $T_{2,B}$ is the bulk time. The magnetization at any time t is given by $M(t) = M_{NU}(t) \cdot M_B(t)$.

In the RW simulation, each fluid particle is placed randomly in the pore space and diffuses in discrete steps across neighboring voxels (Talabi et al., 2009). Whenever the particle hits the solid wall, it is penalized by a factor δ that depends on the surface relaxivity $\delta = 2\Delta\rho/3D$, where Δ is the image voxel resolution and D is the fluid diffusion coefficient (Bergman et al., 1995). There are at least two ways to apply this penalization:

i. Every fluid particle makes the same contribution to the non-uniform magnetization $M_{NU}(t)$. When the walker hits the solid surface, its contribution is reduced by multiplying it by $(1-\delta)$ (Jin et al., 2009)(Tan et al., 2014).
ii. The walker has a probability δ of being flagged as "killed" whenever it hits the surface. At time t, the value of $M_{NU}(0)$ is reduced by a factor N_t/N_0 where N_0 is the total number of walkers and N_t is the number of walkers that have not been killed at time t (Valfouskaya et al., 2006).

We use the first relaxation scheme although the difference of the computational costs and resulting decays associated with both is negligible.

We observe that the digital image representation of the rock sample can only provide a discrete approximation of the pore shapes. This may induce inaccuracies in the estimated decay, as the discretization slightly increases the contact area for the walkers (Jin et al., 2009). However, we restrict the walker's motion to perpendicular directions, as described in (Watanabe and Nakashima, 2002)), obtaining an accurate fit to analytical results, as shown in Fig. 1. In the figure, the numerical results were obtained with the aid our RW implementation employed in a discrete approximation of a sphere with radius twenty-voxel, while the analytical results were obtained with the aid of Eq. (1).

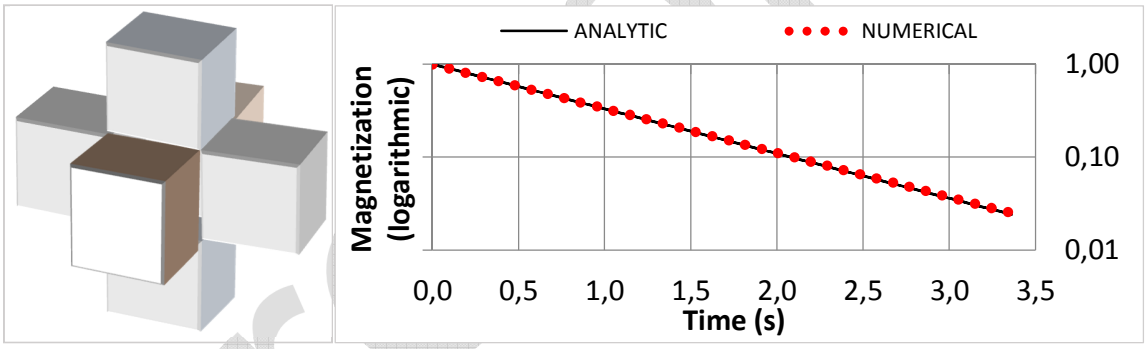

Figure 1. In the Random Walk simulations we restrict the walker's motion to perpendicular directions, obtaining an accurate fit to analytical results (right). The numerical results were obtained with the aid our RW implementation employed in a discrete approximation of a sphere with radius twenty-voxel (radius $20\ um$ and $\Delta = 1\ um$) using $\rho = 5\ um/s$ and $T_2 = 2.8s$, while the analytical results were obtained with the aid of Eq. (1).

The result of the RW simulation is the value of the magnetization $M(t)$ at discrete times $t_k = k\Delta t, k = 1,2, \dots, n$. To interpret the information embedded in this signal, the inverse Laplace transform is applied. This consists of finding the coefficients $c_j, j = 1,2., \dots, m$ that provide the best fit for the relation:

$$M(t_k) = \sum_{j=1}^{m} c_j e^{-\frac{t_k}{T_{2,j}}} \quad . \tag{2}$$

The plot of coefficients c_j as a function of the corresponding times $T_{2,j}$ is typically called the T_2 distribution. Obtaining these coefficients can be stated as a least squares problem and its ill conditioned nature is associated with the presence of noise in the measured signal $M(t)$ (Prange and Song, 2009). Different noise levels associated with the same measurement may result in different T_2 distributions, which may reveal features associated with the noise and not with what was probed in the sample. This effect is limited by the Tikhonov regularization (Day, 2011), which consists of solving the optimization problem:

$$\min_{\boldsymbol{c}} \|\mathbf{Ac} - \mathbf{m}\|^2 + \lambda^2 \|\mathbf{c}\|^2 \,, \tag{3}$$

where $\mathbf{A}$ is a matrix whose entries are given by $A_{k,j} = e^{-\frac{t_k}{T_{2,j}}}$, $\boldsymbol{m}$ is a vector whose entries are the discrete values $M(t_k)$, $\boldsymbol{c}$ is the vector of coefficients c_j, and λ is a regularizer that controls the weight of the solution vector $\boldsymbol{c}$ relative to the minimization of the error $\|\boldsymbol{Ac} - \boldsymbol{m}\|$. In the present work we use the L-curve criterion to determine the regularization value (Hanke, 1996)(Hansen, 1999)(Hansen and O'Leary, 1993).

2.2 - Inverse problem methodology

We state the inverse problem as follows: with the aid of RW simulations performed on the rock sample digital image, determine the surface relaxivity function whose corresponding T_2 distribution best matches the reference (measured) T_2 distribution. If

the surface relaxivity function is parametrized, the inverse problem may be stated as an optimization task in which these parameters must be adjusted.

2.2.1 - Surface relaxivity function parametrization

We benefit from the fact that in a RW simulation the total number of wall collisions of a walker is proportional to the size of the pore in which it resides (the larger the pore is, the smaller the total number of wall collision is, and vice versa), and instead of directly associating a surface relaxivity value with each portion of the solid/fluid interface according to the pore size (which would be impossible in practical implementations), we associate a surface relaxivity value to each total number of wall collisions. In other words, the surface relaxivity $\rho = \rho(\xi)$, where ξ is the total number of wall collisions normalized to the total number of iterations in the RW simulation, as seen in more details in Section 2.2.2.

In the present work, we assume that the surface relaxivity function $\rho(\xi)$ is a linear combination of basic shape functions. We choose Sigmoid shape functions with four parameters to adjust:

$$\rho(\xi) = \sum_{i=1}^{n} A_i + \frac{K_i - A_i}{1 + e^{-B_i(\xi - \xi_i)}} \quad . \tag{4}$$

The values of K_i and A_i control the minimum and maximum values of the sigmoid, the value of ξ_i defines the transition point (from minimum to maximum or vice-versa) and the value of B_i controls the slope of the curve. This choice for the shape functions is suitable to find piecewise continuous functions, establishing $n + 1$ different horizontal relaxivity asymptotes for different pore size intervals. Notably, it would be suitable to approximate

the experimental results found in (Liu et al., 2014), for instance. The sharpness of the relaxivity transitions is controlled by the slope. We limited the number of shape functions here to $n = 2$, reducing our search to 8 optimization parameters. We emphasize that with this choice for the shape function we have increased flexibility and can represent relaxivity functions that either increase or decrease with the pore size, as well as to represent a uniform value, as shown later in Section 3.2. Examples of different surface relaxivity functions, illustrating some of the different tendencies that we can recover using the sum of two Sigmoid functions, are given in Fig. 2.

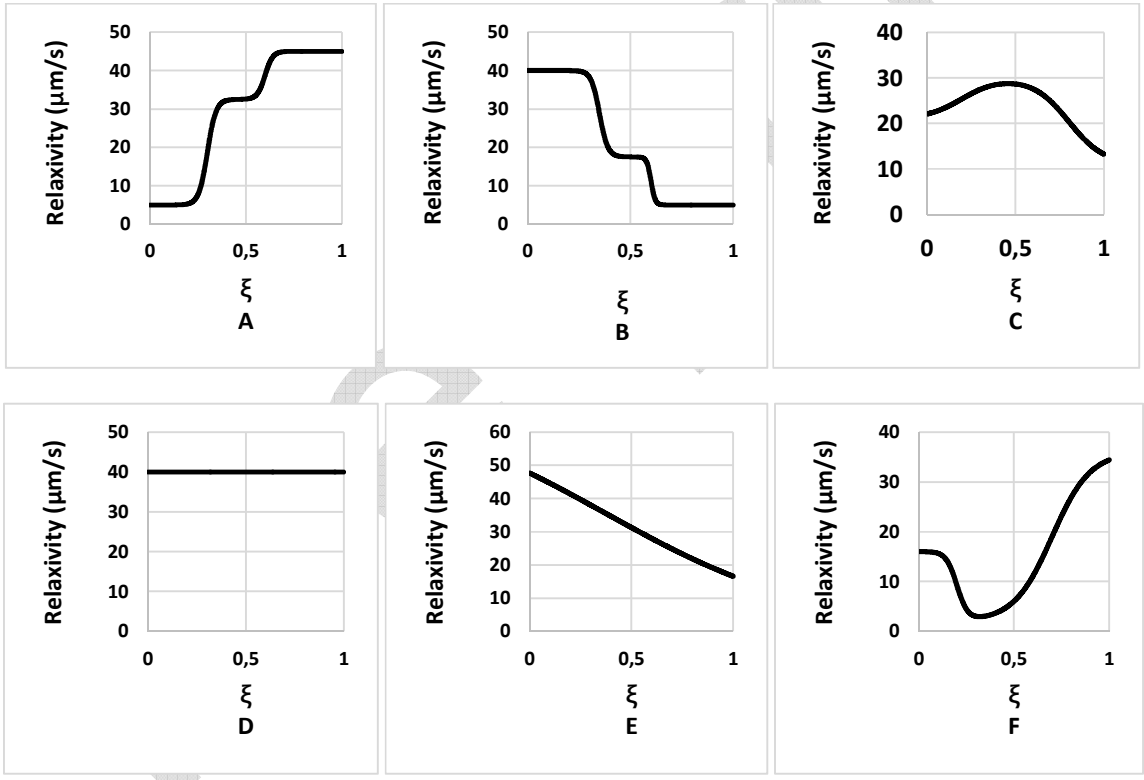

Figure 2. Examples of different surface relaxivity functions, illustrating some of the different tendencies that we can recover using the sum of two Sigmoid functions. The vectors of parameters $(K_1, A_1, \xi_1, B_1, K_2, A_2, \xi_2, B_2)$ are chosen as follows: $A = (30, 2.5, 0.3, 45, 15, 2.5, 0.6, 50)$, $B = (2.5, 15, 0.6, 100, 2.5, 15, 0.35, 50)$, $C = (1, 20, 0.8, 10, 10, 1, 0.2, 10)$, $D = (20, 20, 0.5, 25, 20, 20, 0.2, 900)$, $E = (0.5, 35, 0.25, 2, 0.5, 35, 0.5, 2)$, $F = (35, 1, 0.7, 10, 1, 15, 0.2, 35)$.

We end this section by making two final comments: First, we expect that a distribution of total number of wall collisions (and not a single value) is associated with each pore size (range). This is why we consider the Sigmoid functions for the surface relaxivity function, because it provides the flexibility to associate the same surface relaxivity value to an entire ξ range. Even if the distributions of total number of wall collisions associated with the different pore size ranges partially overlap, we expect that to have a residual impact in the inversion results. This is exactly what the example in Section 3.3 indicates because we could precisely recover the original surface relaxivity function. Second, in principle, in actual rocks, pores of the same size can present different surface relaxivities. Accordingly, assuming that only one exact surface relaxivity value will be associated with each ξ is an idealization, and we make this assumption to formulate a treatable inverse problem. Realistically, we expect that for each pore size range the surface relaxivity value fluctuates around an average value. In that sense, we do not expect that the sum of two Sigmoid functions perfectly fits the actual surface relaxivity variation, but that it well represents the eventual overall tendency of the surface relaxivity to vary with pore size.

2.2.2 - The Mapping Simulation

As we will see next, our inverse method evaluates a candidate function $\rho_c(\xi)$ by executing a RW simulation based on it. To that end, it is crucial to associate a value ξ to each walker. This is done only once, in the beginning of the optimization procedure, with the aid of a preliminary RW simulation, in which every walker is associated with a variable that is increased by 1 whenever it hits a solid wall. At the end of the simulation, we have the normalized set of pairs $\left(k, \frac{y_k}{n_{st}}\right), k = 1, \dots, N$, where N is the total number of walkers, k

is the walker identification, y_k is its corresponding total number of collisions, and n_{st} is the total number of iterations. As mentioned earlier, we define $\xi_k = y_k/n_{st}$. We will refer to this preliminary RW simulation as the Mapping Simulation (MS), because it provides a classifier value ξ to each walker. Notice that no surface relaxivity (or bulk relaxivity) needs to be associated with the pores for the MS. Typically, in the MS we consider $n_{st} = 15{,}000$ for an image resolution of 1μm, which corresponds to around 2.8 seconds (the usual relaxation time measured in the laboratory experiment).

According to what is said above, we note that we assign the same ξ value to walkers that remained the entire time within pores of the same size and to those that visited pores of different sizes, as long as they have had the same number of wall collisions in the MS. It is impossible at this point to precisely predict the impact of this approximation in the inversions, but, according to our preliminary tests, it is residual.

2.2.3 - Shape function optimization

To simulate a random walk decay based on a candidate function $\rho_c(\xi)$ we proceed as follows: We assign to each walker (indexed by k) a relaxivity value ρ_k according to its ξ_k, computed during the MS, i.e., $\rho_k = \rho_C(\xi_k)$. Then, the walker k starts its motion at the same position it started in the MS (carrying its own relaxivity value ρ_k) and is penalized by the factor $\delta = 2\Delta\rho_k/3D$ whenever it hits a solid wall. We perform this with all of the walkers individually and sum the individual magnetization contributions at each time step. At the end of this procedure we have the exponential decay and the corresponding T_2 distribution (applying the inverse Laplace transform to the simulated exponential decay) associated with the function ρ_c.

We use genetic algorithms (GAs) to find the surface relaxivity function whose corresponding simulated T_2 distribution best matches the reference T_2 distribution. We expect them to be robust to treat noisy and incomplete input data, and to reduce the probability of becoming trapped at local minima. The purpose of GAs is to apply environmental pressure (survival of the fittest) to a set of possible solutions to the problem (Eiben and Schoenauer, 2002). In our case, a possible solution (that is typically called an individual) is encoded as a vector of 8 parameters $(K_1, A_1, \xi_1, B_1, K_2, A_2, \xi_2, B_2)$ that characterize the candidate relaxivity function $\rho_C(\xi)$ (see Eq. (4)). For each individual, a RW simulation is performed as described above, and an associated T_2 distribution $\boldsymbol{L^i}$ is obtained. Each individual is then ranked according to the correlation between its associated T_2 distribution and the reference T_2 distribution, i.e., $\boldsymbol{L} \cdot \boldsymbol{L^i}/(\|\boldsymbol{L}\|\|\boldsymbol{L^i}\|)$, where $\boldsymbol{L}$ is the reference T_2 distribution. A perfect match corresponds to a correlation equal to 1.

A common issue in GAs is premature convergence (Pandey et al., 2014). Here, we use a variant of the island methodology to avoid it (Whitley et al., 1998). Our GA implementation divides the population of N individuals (a set of N surface relaxivity functions) in p subpopulations (islands) of the same size N/p. Each of these subpopulations is optimized locally, recombining the information of its individuals using a whole arithmetic operator (described in (Eiben and Smith, 2007)). This recombination is executed in pairs, such that two random individuals $(K_1^1, A_1^1, \dots)$, $(K_1^2, A_1^2, \dots)$ are combined to produce another two individuals $\alpha(K_1^1, A_1^1, \dots) + (1-\alpha)(K_1^2, A_1^2, \dots)$ and $(1-\alpha)(K_1^1, A_1^1, \dots) + \alpha(K_1^2, A_1^2, \dots)$ where α is chosen randomly in the interval $[0, \frac{1}{2}]$. After calculating the correlation of the T_2 distributions associated with these new individuals

with the reference T_2 distribution, the individuals whose associated T_2 distributions result in the poorest correlations are discarded, keeping the subpopulation size constant at each island. This procedure is repeated iteratively, allowing all individuals to recombine only once in each step. After a certain number of iterations g, the individuals with the best correlations migrate to another island. We also apply a mutation operator when the entire island population becomes very similar, i.e., when the relative difference between all individuals is less than 10%. The mutation operator picks one of the individual´s entries and alters it by a randomly chosen percentage in the interval $[0,100]$. In our tests, a population of 48 individuals divided into 4 islands was enough to guarantee convergence after approximately 50 iterations. A probability of 10% for mutation was considered.

3 - Numerical results

3.1 - Effects of surface relaxivity variation

Here we illustrate the effect of the surface relaxivity variation on the T_2 distribution through a synthetic example. A random set of three circular pore families was placed on a white background, as shown in Fig. 3. By pore family, we mean pores within the same size range. A different gray-scale value was associated with each of the families, corresponding to a different relaxivity value (a smaller relaxivity of $5\ \mu m/s$ was associated to the larger pores, a medium relaxivity of $20\ \mu m/s$ was associated to the medium pores and a larger relaxivity of $45\ \mu m/s$ was associated to the smaller pores.) A 2D random walk simulation was performed on this synthetic medium, such that whenever a walker

hits a solid wall, it picked the gray-scale value of the collision pixel, i.e., its magnetization was reduced by the corresponding relaxivity value.

A bulk relaxation time of $T_{2,B} = 2.8s$ and a resolution of $\Delta = 2\ \mu m$ was assumed. A total of $54,575$ walkers were used in the simulation, such that each pixel associated to the pore space received one walker, filling the entire pore space. To simulate noise, we synthetically added white noise to the simulated NMR magnetization decay, such that the signal to noise ratio (SNR) was 368. The SNR here is estimated as $SNR = \frac{\mu_{100}}{\sigma_{100}}$, where μ_{100} is the average of the first 100 decay samples (the first 100 simulated values) and σ_{100} is the standard deviation of the last 100 decay samples. In addition, we used a magnetization threshold stopping criterion value of 0.25%. The same stopping criterion was also used in all the simulations shown in the subsequent sections. The regularization was chosen according to the L-curve criterion.

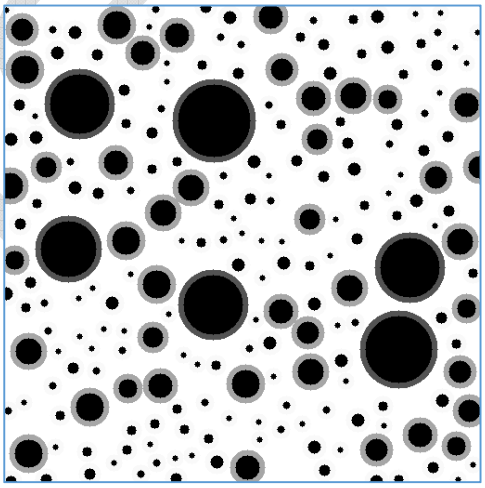

Figure 3. The synthetic medium used in the simulations presented in Sections 3.1, 3.2 and 3.3. A random set of three circular pore families was placed on a white background. A different gray-scale value is associated with each of the pore families. For the simulation presented in Section 3.2, the same relaxivity value was associated with all three families. For the simulation presented in Section 3.3, a different relaxivity value was associated with each of the families.

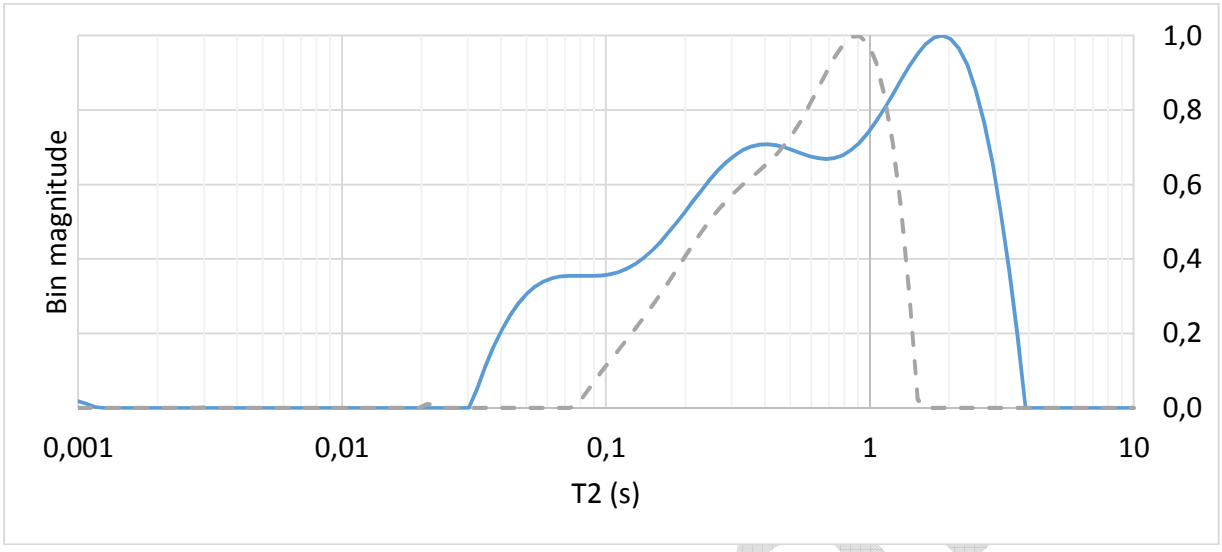

Figure 4. The T_2 distribution obtained from the decay simulated with varying surface relaxivity (continuous line) and the T_2 distribution obtained from the decay simulated with an average uniform surface relaxivity of $20\ \mu m/s$ (dashed line). The two curves are largely different. In particular, the simulation assuming a uniform surface relaxivity produced a predominantly unimodal and narrower T_2 distribution.

The T_2 distribution obtained from the decay simulated with the varying surface relaxivity is shown in Fig. 4 (continuous line). The figure also shows the T_2 distribution obtained from the decay simulated with an average uniform surface relaxivity of $20\ \mu m/s$ (dashed line), i.e., the average uniform surface relaxivity of $20\ \mu m/s$ was associated with all the three pore families. The two relaxation curves are largely different for the same pore size distribution. In particular, the simulation assuming the average uniform surface relaxivity produced a predominantly unimodal and narrower T_2 distribution. The T_2 distribution is narrower for the uniform relaxivity case because, *at the larger pores*, the relaxation occurs more rapidly in the uniform relaxivity case than in the varying relaxivity case (because of the considered surface relaxivities.) Therefore, the portion of the T2 distribution at the right (the part associated with the larger pores) is narrower for the

uniform relaxivity case than for the varying relaxivity case (we recall that relaxation time increases to the right). On the other hand, *at the smaller pores*, the relaxation occurs more slowly in the uniform relaxivity case than in the varying relaxivity case (again, because of the considered surface relaxivities). Therefore, the portion of the T2 distribution at the left (the part associated with the smaller pores) is again narrower for the uniform case than for the varying case. As a result, the T2 distribution as a whole is narrower for the uniform case then for the varying case.

This is an example of how erroneous or incomplete assumptions regarding the surface relativity can affect the NMR simulation. The effect of varying surface relaxivity on petrophysical deliverables derived from NMR relaxation distributions has been discussed in other works (e.g. (Arns et al., 2006) and (Ryu, 2008)).

3.2 - Synthetic case with uniform relaxivity

We now evaluate the performance of our method to estimate the surface relaxivity for the uniform relaxivity case. For this purpose, we associate $\rho = 20\ \mu m/s$ with all the three pore families shown in Fig. 3. Our reference T_2 distribution comes from a RW simulation executed, again, with 54,575 walkers (filling the entire pore space). To check the robustness of the method for noisy input data, we considered two different SNRs in the simulated decay, a SNR of 298, compatible with NMR experiments performed in the lab (Fig. 5), and a SNR of 31, compatible with logging operations (Fig. 6). In Figs. 5(A) & 6(A) we show the surface relaxivity function obtained with the aid of our method and in Figs. 5(B) & 6(B) we show the match of the resulting simulated T_2 distribution with the

reference. A total of 148 generations were iterated (in general, each optimization took approximately 30 generations to converge).

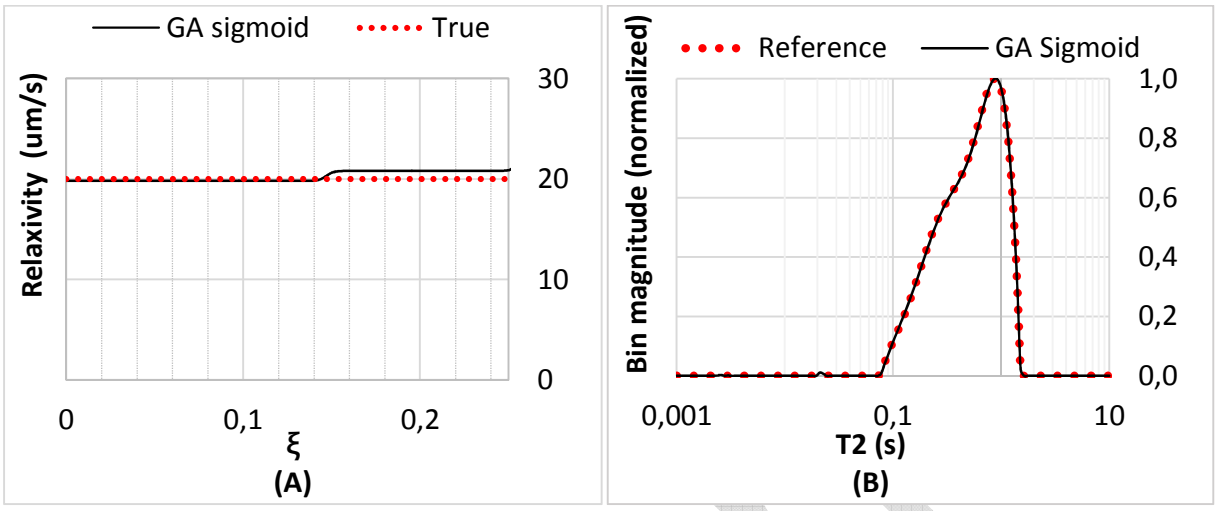

Figure 5. (A) Comparison between the surface relaxivity function obtained from the inversion procedure and the "true" one. (B) The corresponding T_2 distributions. The SNR considered here is 298, which is compatible with NMR experiments performed in the lab. $\lambda = 0.11$

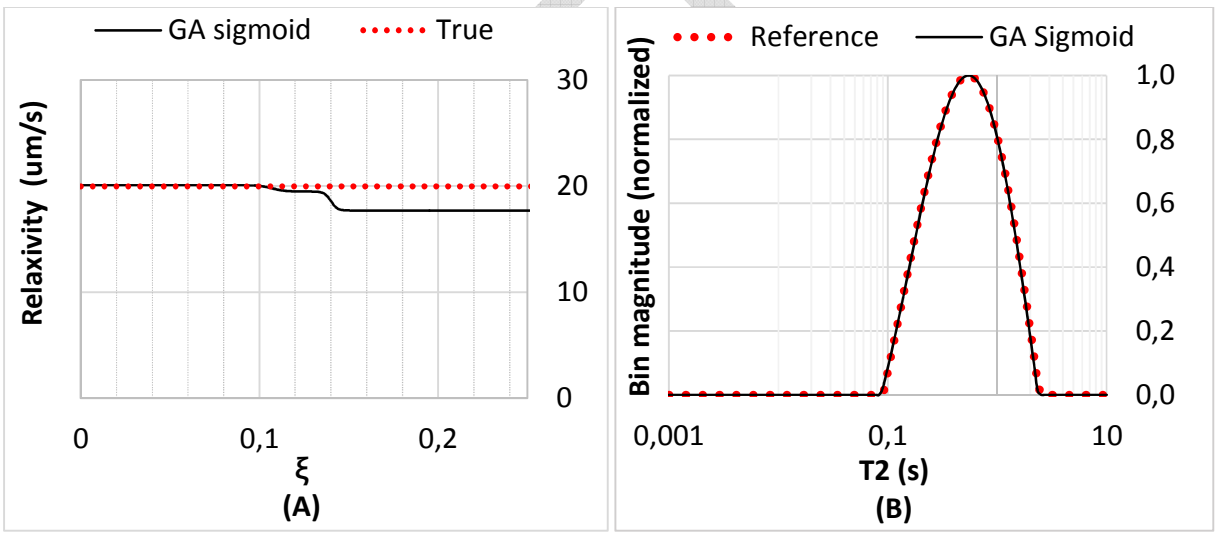

Figure 6. (A) Comparison between the surface relaxivity function obtained from the inversion procedure and the "true" one. (B) The corresponding T_2 distributions. The SNR considered here is 31, which is compatible with NMR logging operations. $\lambda = 3.19$

The results validate our implementation and show that our method performs well for the uniform relaxivity case, where the obtained two-sigmoid combination adapted very well to the uniform relaxivity value even for the noisiest case. We repeated each inversion 4 times and obtained the same results, indicating that the problem has only one global minimum.

3.3 - Synthetic case with varying relaxivity

The second test corresponds to the scenario in Section 3.1, i.e., the medium is represented in Fig. 3 and a different surface relaxivity value was associated with each of the three pore families

. In Figs. 7(A) & 8(A) we compare the surface relaxivity function estimated with the aid of our method with the original surface relaxivity variation (continuous line vs. dotted line), while in Figs. 7(B) & 8(B) we show the match between the resulting T_2 distribution and the reference. For Fig. 7, we have considered a SNR of 338, compatible with NMR experiments performed in the lab, while for Fig. 8, we have considered a SNR of 32, compatible with logging operations. As in the previous section, we repeated each inversion 4 times and obtained the same results, indicating that the problem has only one global minimum. The figures show that the method performed well even for the noisiest case, validating both methodology and implementation. In addition, a uniform surface relaxivity value does not exist that results in a good match for the reference T_2 distribution. This is clearly shown by the dashed curves in Figs. 7(B) & 8(B). We emphasize that the uniform surface relaxivity value used for each figure was also determined from an optimization procedure, i.e., there is no other uniform surface relaxivity value that results in a better match for the reference T_2 distribution than those shown in Figs. 7(A) and 8(A).

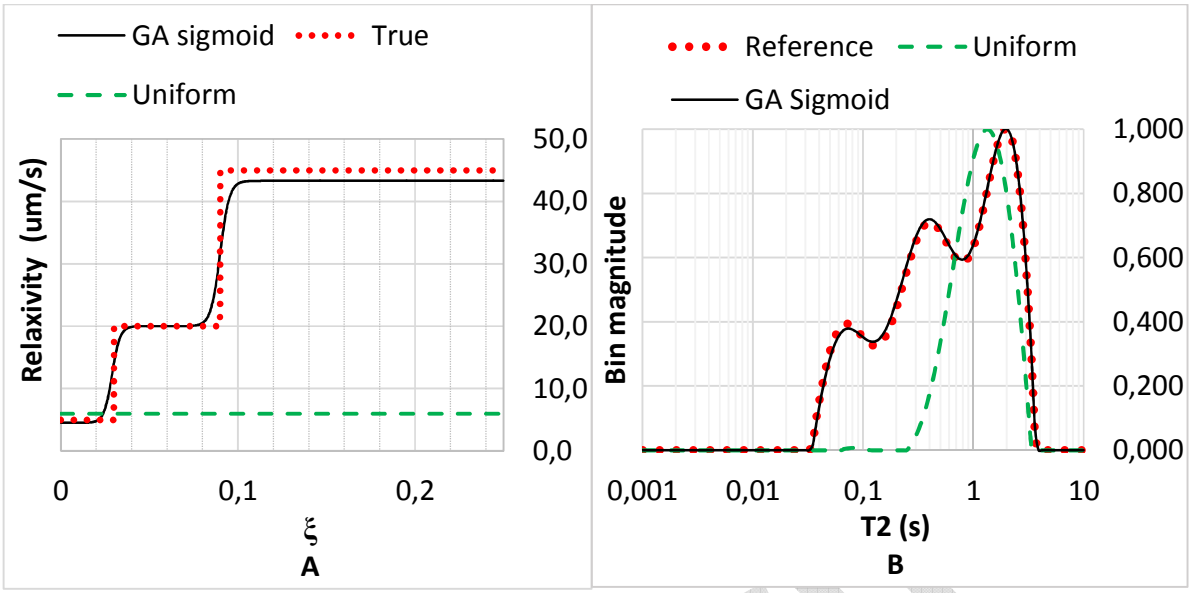

401

402 **Figure 7. (A) Comparison between the surface relaxivity function obtained from the inversion procedure and**
403 **the "true" one. (B) The corresponding T_2 distributions. The SNR considered here is 338, which is compatible**
404 **with NMR experiments performed in the lab. The T_2 distribution corresponding to the uniform relaxivity**
405 **represented in (A) is also plotted in (B). $\lambda = \frac{1}{2}$**

406

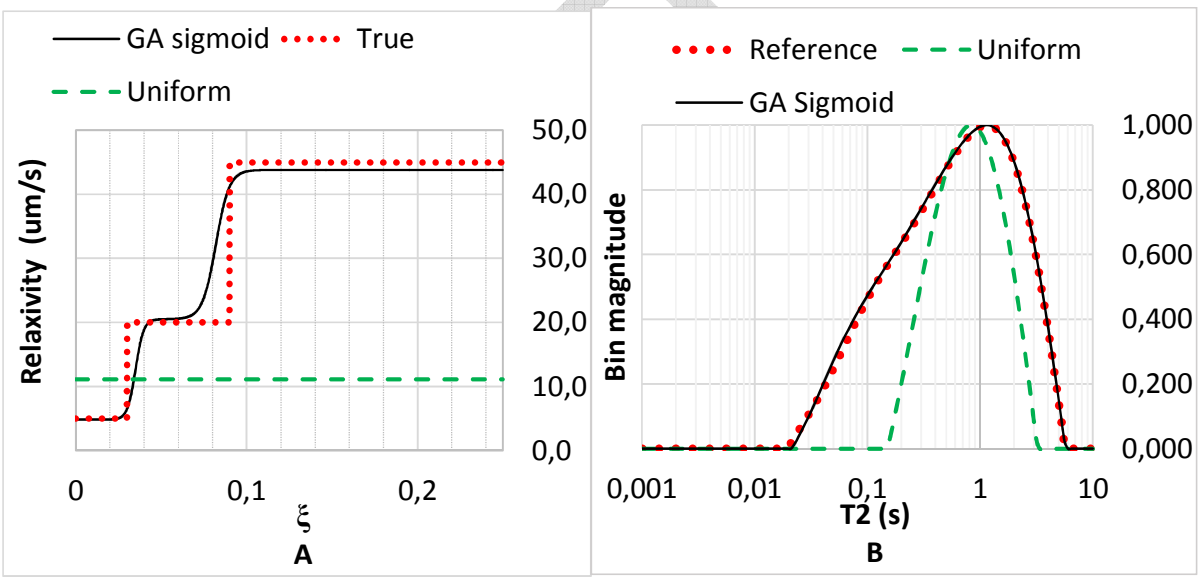

407

408 **Figure 8. (A) Comparison between the surface relaxivity function obtained from the inversion procedure and**
409 **the "true" one. (B) The corresponding T_2 distributions. The SNR considered here is 32, which is compatible**
410 **with logging operations. The T_2 distribution corresponding to the uniform relaxivity represented in (A) is also**
411 **plotted in (B). $\lambda = 3.06$.**

3.4 - Laboratory case

Now we apply the developed methodology to an actual sedimentary rock core. The reference T_2 distribution is now the actual T_2 distribution from the lab. We also compare the obtained results with the experimental determination of an average (uniform) effective transverse surface relaxivity. The chosen sample is a calcite limestone outcrop, Edwards White (EW), from the Edwards Formation located in the central-west state of Texas (USA), with gas porosity and permeability of 0.28 and $5.5\ mD$, respectively (Silva Jr et al., 2015). A slice of the sample tomographic image is shown in Fig. 9.

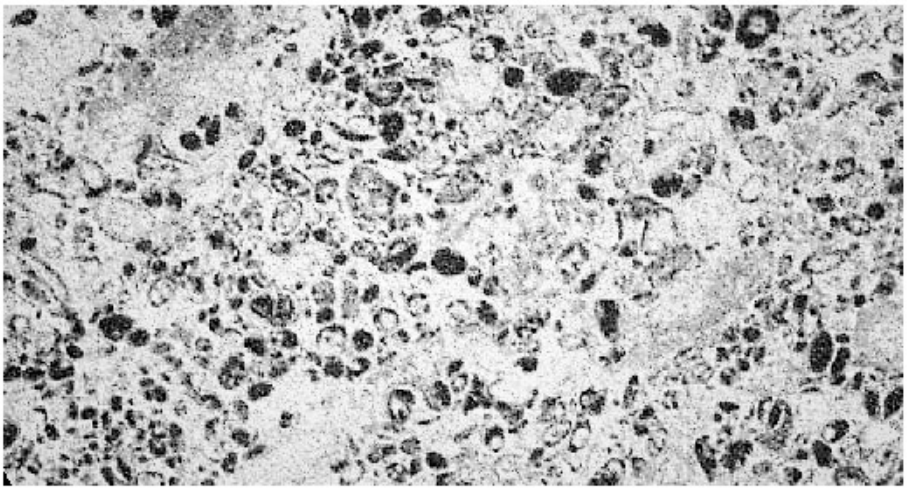

Figure 9. A slice of the Edwards White's tomographic image.

In the laboratory, an average effective relaxivity can be calculated from the two dimensional NMR experiment called $D - T_2$ (diffusion coefficient T_2), a technique that measures the correlation between both parameters (Souza et al., 2013)(Zielinski et al., 2010). Fig. 10 shows the $D - T_2$ map signal (contour lines) of the EW core. The experimental details of the NMR technique used to acquire the T_2 data and to perform the $D - T_2$ are outside the scope of this work and can be found in (Luo et al., 2015)(Souza et

al., 2013) (Zielinski et al., 2010). From the $D - T_2$ experiment, we determined an average uniform surface relaxivity of $15\ \mu m/s$.

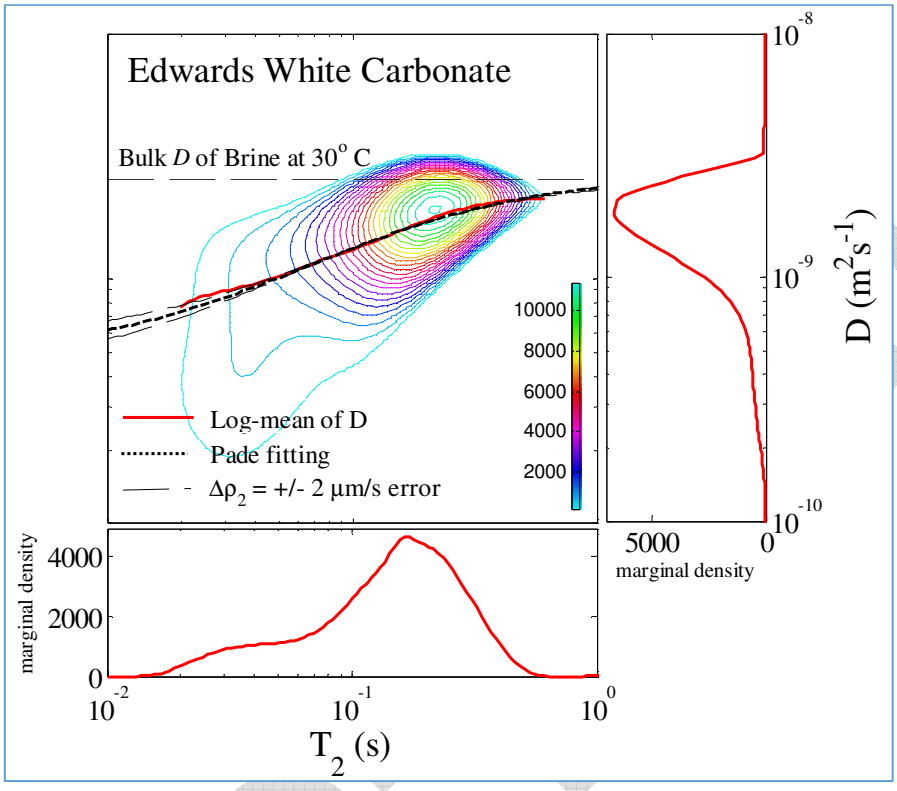

Figure 10. 2D NMR $D - T_2$ map of the Edwards White sample, showing the Padé fitting (black dotted line) that resulted in an effective $\rho_2 = 15\ \mu m/s$. Additional fittings (black dashed lines) considering the error on the input parameters: cementarion coefficient (m) and bulk diffusion coefficient D_0. The estimated error determined was $\Delta\rho_2 = \pm 2\ \mu m/s$. All the fittings were performed considering the average of D for each T_2 bin.

The SNR of the decay signal measured in the lab was estimated at 378. In Fig. 11, we show the surface relaxivity function estimated with the aid of our method, and in Fig. 12, we show the match between the resulting and measured T_2 distribution. As in the previous sections, we repeated the inversion 4 times and obtained the same results, indicating that the problem has only one global minimum. In Fig 12, we also plot the T_2

distribution resulting from a RW simulation performed with the uniform relaxivity of $\rho = 15\ \mu m/s$ (the value estimated in the lab.)

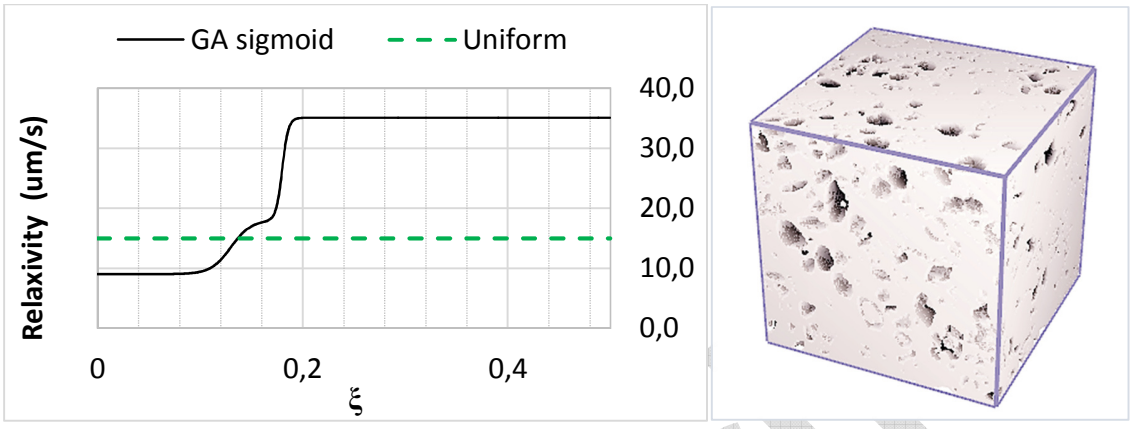

Figure 11. Edwards White's surface relaxivity function obtained from the inversion procedure. The surface relaxivity magnitude decreases with pore size. More specifically, the obtained relaxivity function suggests the existence of (approximately) two different horizontal relaxivity asymptotes associated with two different pore size intervals. The SNR of the measured NMR decay signal was estimated at 378.

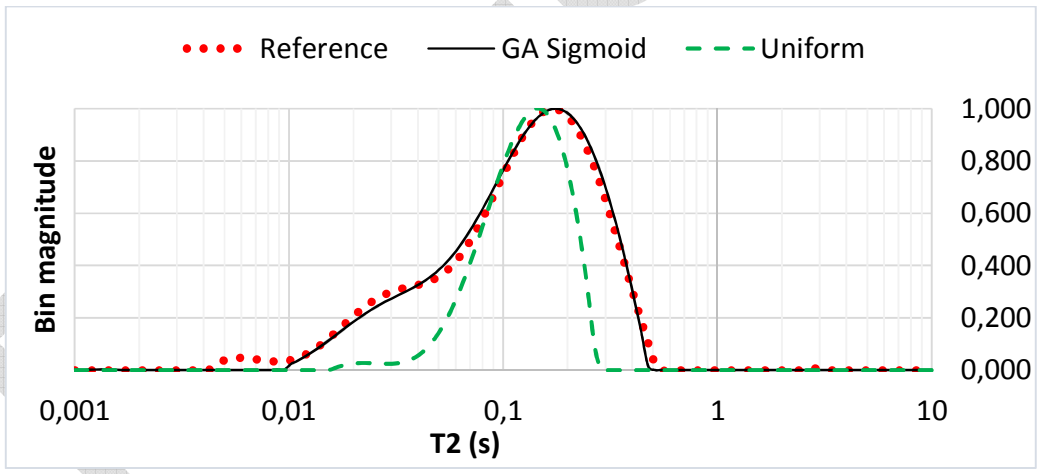

Figure 12. Comparison between the T_2 distribution corresponding to the surface relaxivity function shown in Fig. 11 and the T_2 distribution measured in the lab. The T_2 distribution corresponding to the uniform relaxivity of $15\ \mu m/s$ (the relaxivity value obtained from the $D - T_2$ experiment) is also plotted in the figure. $\lambda = 0.19$

455 The results shown in Fig. 11 indicate that the magnitude of the surface relaxivity
456 decreases as the pore size increases. More specifically, the obtained surface relaxivity
457 function suggests the existence of (approximately) two different horizontal relaxivity
458 asymptotes associated with two different pore size intervals. In addition, Figure 12Fig. 12
459 shows that the relaxivity function shown in Fig. 11 leads to a T_2 distribution that accurately
460 matches the reference. In fact, it matches the reference much more precisely than the T_2
461 distribution obtained with the uniform surface relaxivity value of $15\ \mu m/s$. In that sense,
462 we truly believe that the relaxivity function obtained with the aid of the proposed
463 methodology is a better estimate for the surface relaxivity, for any practical implication,
464 than the uniform value obtained from the $D - T_2$ experiment. The T_2 distribution obtained
465 with the aid of the proposed method does not match well the reference only in a small
466 portion at the left, related to the relaxation at the smallest pores. We can think of some
467 potential explanations for this local mismatch. First, the digital image may not have
468 captured accurately the micro-porosity (we recall here that the gas porosity is 28% while
469 the porosity digitally calculated from the tomographic image is approximately 20.5%).
470 Second, the physical dimensions of the image in which we performed the RW are shorter
471 than the physical dimensions of the sample used in the NMR experiment. In that sense,
472 the image used may not be a perfect representative volume. Third, there are methodology
473 approximations, as mentioned previously in the text, that can impact the inversion results.
474 Currently, it is impossible to know for sure the reason for the small local mismatch.

475 We end this section providing a final comment. In principle, the degree of correlation
476 between the simulated T_2 distribution and the reference T_2 distribution may be indicative
477 of the error associated with the obtained surface relaxivity function. However, more tests

need to be performed before we can make that statement. It certainly would be valuable to check the inversion result's accuracy and, for each case, determine if the surface relaxivity variation is indeed linked to the pore size.

4 - Summary and conclusions

In the present work we formulated and solved an inverse problem to recover the surface relaxivity as a function of pore size. The input data for our technique are the T_2 distribution measurement and the micro-tomographic image of the rock sample under investigation. We simulate the NMR signal relaxation for a given surface relaxivity function using the random walk method, and the optimization is performed using genetic algorithms, where we find the surface relaxivity function that leads to the best match for the T_2 distribution measurement. In the developed methodology, we use the link between pore size and total number of wall collisions in the random walk simulations.

We evaluate the proposed method's performance using inversions from (noisy) synthetic and laboratory input data. The SNRs are compatible with lab experiments and field log measurements. Regarding the results obtained from synthetic input data, the method could accurately recover the original surface relaxivity function for the case of uniform relaxivity as well as for the case of varying relaxivity, for both SNR levels. Regarding the results obtained from the laboratory input data, we verified that we could precisely match the measured T_2 distribution. On the other hand, the T_2 distribution resulting from the uniform relaxivity assumption did not accurately match the measured T_2 distribution. This indicates that the relaxivity function obtained using the proposed

method is presumably a better estimate, for any practical implication, than the uniform value obtained from the $D - T_2$ experiment. In principle, the degree of correlation between the simulated T_2 distribution and the reference T_2 distribution may be indicative of the error associated with the obtained surface relaxivity function. However, more tests need to be performed before we can make that statement. It would be valuable to check the inversion result's accuracy and, for each case, determine if the surface relaxivity variation is linked to pore size.

Acknowledgements

This work was carried out in association with the ongoing NMR Project, sponsored by Shell, registered as "Aplicação de técnicas avançadas de Ressonância Magnética Nuclear (RMN) assistidas por ferramentas computacionais na avaliação petrofísica de rochas carbonáticas" (ANP 18999-3) under the ANP R&D levy as "Compromisso de Investimentos com Pesquisa e Desenvolvimento". The authors also recognize the support from CAPES, CNPq and FAPERJ. F. B. recognizes the support from National University of Costa Rica (UNA).

References

Arns, C.H., Sheppard, A.P., Saadatfar, M., Knackstedt, M.A., others, 2006. Prediction of permeability from NMR response: surface relaxivity heterogeneity, in: SPWLA 47th Annual Logging Symposium. Society of Petrophysicists and Well-Log Analysts.

Bergman, D.J., Dunn, K.-J., Schwartz, L.M., Mitra, P.P., 1995. Self-diffusion in a periodic porous medium: A comparison of different approaches. Phys. Rev. E 51, 3393–3400.

522 Boggs, S., 2009. Petrology of Sedimentary Rocks. Cambridge University Press., pp. 137–
523 206.

524 Brownstein, K.R., Tarr, C.E., 1979. Importance of classical diffusion in NMR studies of
525 water in biological cells. Phys. Rev. A 19, 2446–2453.

526 Coates, G.R., Xiao, L., Prammer, M.G., 1999. NMR logging: principles and applications.
527 Haliburton Energy Services.

528 Day, I.J., 2011. On the inversion of diffusion NMR data: Tikhonov regularization and
529 optimal choice of the regularization parameter. Journal of Magnetic Resonance
530 211, 178–185.

531 Dunn, K.-J., Bergman, D.J., Latorraca, G.A., 2002. Nuclear magnetic ressonance:
532 Petrophysical and Logging applications. Pergamon. Handbook of geophysical
533 exploration. Volume 32.

534 Eiben, A.E., Schoenauer, M., 2002. Evolutionary computing. Information Processing
535 Letters 82, 1–6.

536 Eiben, A.E., Smith, J.E., 2007. Introduction to Evolutionary Computing, in:
537 NaturalComputingSeries. Springer Berlin Heidelberg. Ch: 3.5, pp. 42–69.

538 Hanke, M., 1996. Limitations of the L-curve method in ill-posed problems. BIT Numerical
539 Mathematics 36, 287–301.

540 Hansen, P.C., 1999. The L-curve and its use in the numerical treatment of inverse
541 problems. IMM, Department of Mathematical Modelling, Technical University of
542 Denmark.

543 Hansen, P.C., O'Leary, D.P., 1993. The Use of the L-Curve in the Regularization of
544 Discrete Ill-Posed Problems. Siam Journal on Scientific Computing 14.

545 Jin, G., Torres-Verdín, C., Toumelin, E., 2009. Comparison of NMR simulations of porous
546 media derived from analytical and voxelized representations. Journal of Magnetic
547 Resonance 200, 313–320.

548 Keating, K., Knight, R., 2012. The effect of spatial variation in surface relaxivity on nuclear
549 magnetic resonance relaxation rates. Geophysics 77, E365–E377.

550 Liu, H., d Eurydice, M.N., Obruchkov, S., Galvosas, P., 2014. Determining pore length
551 scales and pore surface relaxivity of rock cores by internal magnetic fields
552 modulation at 2 MHz NMR. Journal of Magnetic Resonance 246, 110–118.

553 Looyestijn, W.J., Hofman, J., 2006. Wettability-index determination by nuclear magnetic
554 resonance. SPE Reservoir Evaluation & Engineering 9, 146–153.

555 Luo, Z.-X., Paulsen, J., Song, Y.-Q., 2015. Robust determination of surface relaxivity from
556 nuclear magnetic resonance DT2 measurements. Journal of Magnetic Resonance
557 259, 146–152.

558 Pandey, H.M., Chaudhary, A., Mehrotra, D., 2014. A comparative review of approaches
559 to prevent premature convergence in GA. Applied Soft Computing 24, 1047–1077.

560 Prange, M., Song, Y.-Q., 2009. Quantifying uncertainty in NMR spectra using Monte Carlo
561 inversion. Journal of Magnetic Resonance 196, 54–60.

562 Ryu, S., 2008. Effects Of Spatially Varying Surface Relaxivity And Pore Shape On Nmr
563 Logging. Society of Petrophysicists and Well-Log Analysts, SPWLA-2008-BB CP.

564 Saidian, M., Prasad, M., 2015. Effect of mineralogy on nuclear magnetic resonance
565 surface relaxivity: A case study of Middle Bakken and Three Forks formations. Fuel
566 161, 197–206.

567 Silva Jr, G.P. da, Franco, D.R., Stael, G.C., Oliveira Lima, M. da Costa de, Martins, R.S.,
568 Moraes França, O. de, Azeredo, R.B.V., 2015. Petrophysical studies of north
569 American carbonate rock samples and evaluation of pore-volume compressibility
570 models. Journal of Applied Geophysics 123, 256–266.

571 Souza, A., Carneiro, G., Zielinski, L., Polinski, R., Schwartz, L., Hürlimann, M.D., Boyd,
572 A., Rios, E.H., Santos, B.C.C. dos, Trevizan, W.A., others, 2013. Permeability
573 Prediction Improvement Using 2D NWR Diffusion-T2 Maps, in:
574 SPWLA54thAnnualLoggingSymposium. Society of Petrophysicists and Well-Log
575 Analysts.

576 Talabi, O., AlSayari, S., Iglauer, S., Blunt, M.J., 2009. Pore-scale simulation of NMR
577 response. Journal of Petroleum Science and Engineering 67, 168–178.

578 Tan, M., Xu, J., Zou, Y., Xu, C., 2014. Nuclear magnetic resonance (NMR) microscopic
579 simulation based on random-walk: Theory and parameters analysis. Journal of
580 Central South University 21, 1091–1097.

581 Valfouskaya, A., Adler, P.M., Thovert, J.-F., Fleury, M., 2006. Nuclear magnetic
582 resonance diffusion with surface relaxation in porous media. Journal of Colloid and
583 Interface Science 295, 188–201.

584 Watanabe, Y., Nakashima, Y., 2002. RW3D. m: three-dimensional random walk program
585 for the calculation of the diffusivities in porous media. Computers & geosciences
586 28, 583–586.

587 Whitley, D., Rana, S., Heckendorn, R.B., 1998. The Island Model Genetic Algorithm: On
588 Separability, Population Size and Convergence. Journal of Computing and
589 Information Technology 7, 33–47.

590 Zielinski, L., Ramamoorthy, R., Minh, C.C., Al Daghar, A., Abdelaal, A.., 2010. Restricted
591 diffusion effects in saturation estimates from 2D Diffusion-Relaxation NMR maps.
592 Annual Technical Conference and Exhibition of Society of Petroleum Engineers
593 134841.

594